Key Engineering Materials
ISSN: 1662-9795, Vol. 1050, pp 69-80
doi:10.4028/p-1eNlcu

Submitted: 2026-01-16
Revised: 2026-02-18
Accepted: 2026-02-18
Online: 2026-04-16

Parameter Optimization and Data-Driven Soft-Sensor Framework for Torque Prediction in Bobbin-Tool Friction Stir Welding of AA2024

Fares Nouira[1,a*], Luciano Bergmann[1, b], Frederic E. Bock[1,c], Ghada Bouattour[2,d], Marco Pacchione[3,e] and Benjamin Klusemann[1,2,f]

[1]Helmholtz-Zentrum Hereon, Institute of Material and Process Design, 21502 Geesthacht, Germany

[2]Leuphana University Lüneburg, Institute for Production Technology and Systems, 21335 Lüneburg, Germany

[3]Airbus, OMTMW – Manufacturing Engineering R&T, 21129 Hamburg, Germany

[a]fares.nouira@hereon.de, [b]luciano.bergmann@hereon.de, [c]frederic.bock@hereon.de, [d]ghada.bouattour@leuphana.de, [e]marco.pacchione@airbus.com, [f]benjamin.klusemann@hereon.de

Keywords: Bobbin-Tool Friction Stir Welding, Process Parameter Optimization, Soft-Sensor Framework, Torque Prediction, Machine Learning, Aerospace Aluminum Alloys, Process Monitoring.

Abstract. Bobbin-Tool Friction Stir Welding (BT-FSW) is a solid-state joining process in which axial forces are internally balanced by the tool, eliminating the need for a backing plate and enabling the joining of hollow aerospace structures. Owing to the coupled thermo-mechanical nature of the process, weld stability and quality are governed by the interaction between process parameters and the resulting torque response, which is difficult to assess in situ using conventional sensing alone. BT-FSW experiments were performed on AA2024-T351 sheets with thicknesses of 2.4, 2.8 and 3.6 mm using a structured Design of Experiments (DoE). The 3.6 mm joints achieved approximately 90 % of the base-material strength, while the 2.4 and 2.8 mm joints reached about 80 % and 85 %, respectively. These mechanical results were used as ground truth to train machine learning regression models for steady-state torque predictions. By augmenting nominal process parameters with force-derived features, the proposed soft-sensing framework achieved strong agreement between predicted and measured torque, demonstrating that compact, physics-based feature engineering enables reliable prediction under limited experimental data conditions.

Introduction

Bobbin-Tool Friction Stir Welding (BT-FSW) is a self-reacting variant of friction stir welding (FSW) in which opposing shoulders generate a balanced thermal field without backing support. Compared to conventional FSW, this configuration minimizes distortion, eliminates the single-sided probe exit keyhole and significantly reduces the risk of lack of penetration due to the symmetric loading condition, making BT-FSW attractive for lightweight aerospace structures where geometric accuracy and joint integrity are critical **[1, 2]**. The coupled thermo-mechanical nature of the process makes it highly sensitive to the interaction between rotational speed, traverse speed, and axial loading, which jointly govern frictional heating, material flow, and material consolidation.

In aluminum alloys, the consequences of heat input and stirring stability on nugget morphology, hardness evolution and tensile properties after FSW are well established **[3, 4]**. Macroscopic indicators, such as onion-ring structures, joint-line remnants and localized softening have been linked to unstable flow and incomplete consolidation, and torque signatures have been used as an in-process indicator of these conditions **[5]**. Consequently, torque provides a practical proxy for the instantaneous process state in both FSW and BT-FSW.

Despite this relevance, most BT-FSW investigations remain limited to single-thickness configurations or rely on qualitative interpretation of torque signals, and comprehensive multi-thickness datasets combining synchronized process signals with mechanical and macrostructural validation are scarce. In parallel, machine-learning-based soft sensors have been increasingly

explored in manufacturing and forming processes to estimate unmeasured process states. Nadeau et al. **[6]** demonstrated early regression-based surrogate models for process response prediction, highlighting the potential of data-driven approaches under constrained experimental datasets. Belalia et al. **[7]** extended such concepts using signal-based features for process monitoring, while Bock et al. **[8]** proposed physics-guided soft-sensor frameworks that explicitly combine process knowledge with machine learning to improve robustness and interpretability in forming applications. Penalva et al. **[9]** investigated data-driven and hybrid modeling strategies with a stronger reliance on numerical process descriptions. More recently, Bock et al. **[10]** demonstrated that machine-learning-based surrogate models informed by mechanical principles can achieve reliable predictions while maintaining physical consistency, reinforcing the relevance of physics-aligned soft sensors for complex thermo-mechanical processes. However, the transfer of such validated soft-sensor concepts to BT-FSW, particularly across varying sheet thicknesses and under realistic experimental data constraints, remains largely unexplored.

Soft sensors are increasingly used in manufacturing to estimate unmeasured process states from indirect sensor signals, particularly where direct measurement is impractical or costly **[11]**. In welding applications, however, most reported soft sensors rely on large datasets and highly nonlinear black-box models, offering limited physical interpretability. For BT-FSW, where experimental data are inherently scarce, this creates a gap between predictive accuracy and physical understanding.

The present work addresses this gap by developing an interpretable, physics-aligned soft-sensing framework based on supervised regression in which physical process understanding guides feature selection and target definition, enabling robust data-driven prediction under limited data availability. Therefore, a structured multi-thickness investigation of BT-FSW on AA2024-T351 sheets with thicknesses of 2.4, 2.8, and 3.6 mm has been performed. The central objective of this work is the prediction of steady-state torque as a soft-sensor output. Although torque is directly measurable in BT-FSW, its prediction is not pursued as an end in itself. Instead, torque prediction is used as a physically meaningful intermediate soft sensor that links process parameters and force signals to the underlying thermo-mechanical process state, enabling process understanding, process planning, and the identification of anomalous or unstable welding conditions. At first, a DoE is employed to study the combined influence of rotational speed, traverse speed, and gap force on torque evolution and weld quality. Mechanical characterization through tensile testing, macrostructural inspection, and hardness mapping provides ground-truth indicators of the weld performance. Building on these data, the proposed framework is used to predict steady-state torque using process parameters and measured force signals as inputs, providing a quantitative basis for torque-based process monitoring and stability assessment in BT-FSW.

Proposed Approach and Methodology

The objective of this study is to develop a soft-sensing approach for predicting steady-state torque in BT-FSW from measured process parameters and force signals under limited experimental data availability. An integrated workflow is implemented in which welding trials, data acquisition, mechanical characterization, and supervised regression are combined into a single analysis pipeline, see Fig. 1.

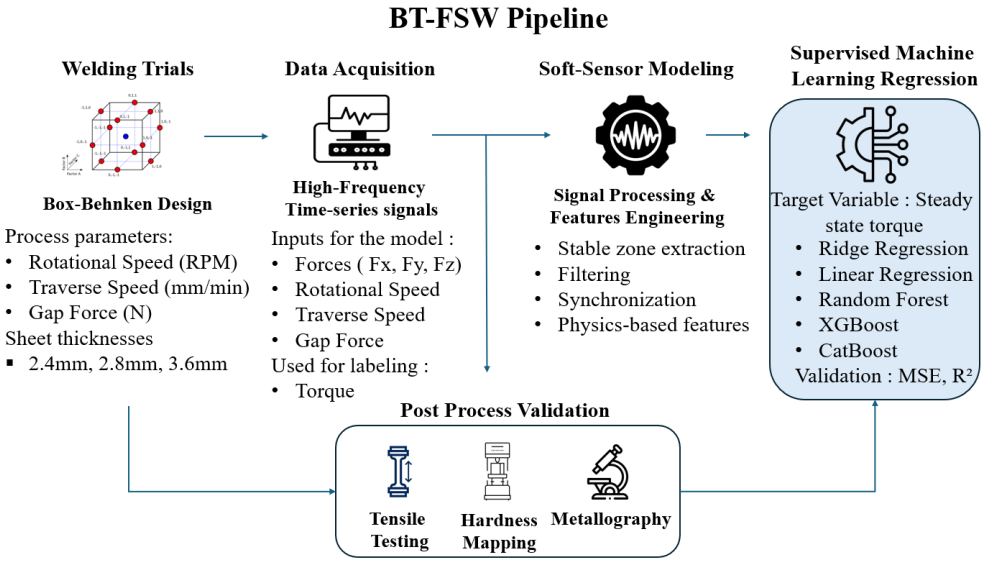

Fig. 1 Process workflow used in this study.

Within this workflow, BT-FSW experiments are conducted under controlled conditions, relevant process and force signals are recorded, joints are mechanically and microstructurally evaluated, and the resulting dataset is used to train and validate regression models constituting the soft sensor.
The experimental design followed a Box–Behnken DoE for each thickness, systematically varying rotational speed ($\mathbf{n_{rot}}$), traverse speed ($\mathbf{v}$) and gap force ($\mathbf{F_g}$) over three thicknesses, see Table1. This design efficiently captures main, quadratic and interaction effects while limiting the number of trials **[12]**.

Table 1 DoE parameter ranges investigated for the different thicknesses.

Thicknesses (mm)	Rotational Speed (RPM)	Traverse Speed (mm/min)	Gap Force (N)
2.4	250–300–350	100–150–200	1500–2000–2500
2.8	300–350–400		
3.6			

Materials and Process. All welds were produced on a Tricept T805 parallel-kinematic robot equipped with a semi-stationary bobbin tool consisting of two opposing shoulders connected by a threaded probe, with the upper shoulder held stationary relative to the machine frame and the lower shoulder rotating with the spindle. The clamping arrangement and welding workspace are shown in Fig. 2, including the positioning of reference strips, side bosses, spike pads and retainers used for specimen fixation.

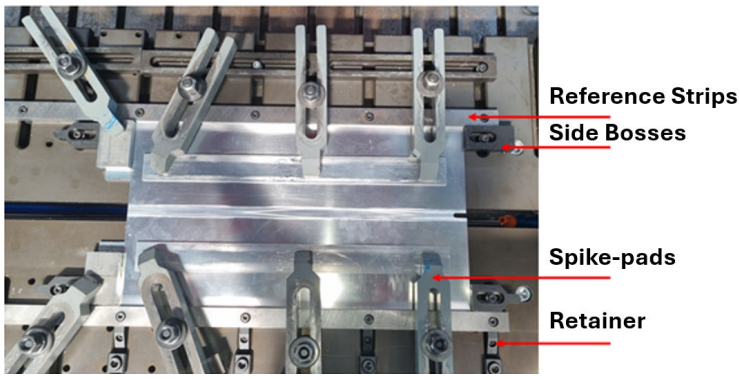

Fig. 2 Experimental clamping setup used during BT-FSW, ensuring stable positioning and force-controlled welding conditions.

The base material plates were locally machined in the welding region to achieve the target joint thicknesses of 2.4, 2.8, and 3.6 mm, starting from initial plate thicknesses of 3.2, 3.5, and 4.5 mm, respectively.
Welding was performed in force-controlled mode, with axial gap force regulated through a closed-loop system to maintain stable tool–workpiece contact. Rotational speed and traverse speed were controlled via a Siemens NC unit. Welds were executed according to DIN EN ISO 25239 along the rolling direction over a length of 550 mm to ensure a fully developed steady-state region suitable for mechanical sampling and sensor assessment.
After welding, each weld was sectioned into 16 transverse slices following the layout in Fig. 3. Cuts 10–12 were allocated for tensile testing, Cut 3 for macrostructural inspection and Barker-etched microscopy, and Cut 16 for macrostructural inspection and hardness mapping. For each thickness, 15 welds were produced, yielding 45 structured experiments.

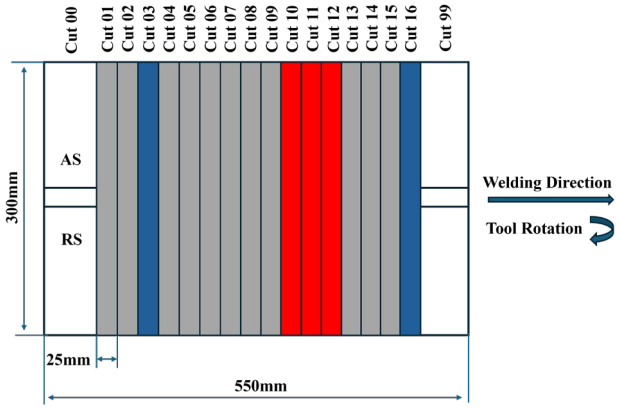

Fig. 3 Cutting layout used for specimen extraction, indicating the advancing side (AS), retreating side (RS), welding direction (identical to rolling direction) and the locations of cuts.

Mechanical Characterization. Tensile tests were performed on three parallel-gauge specimens per weld, using a 150 mm gauge length and a 50 mm extensometer, under displacement control at 1 mm/min. This configuration follows established tensile evaluation practices for friction-stir-welded aerospace alloys, where parallel specimens reliably capture joint efficiency without requiring dog-bone machining **[13]**. Macrostructural observations were conducted on polished sections from Cut 3 using a VHX digital microscope at 50× magnification, and Barker-etched micrographs revealed nugget morphology, flow lines and joint-line remnants (JLR) **[14]**. Hardness profiles from Cut 16 were measured using Vickers HV0.1 with 0.5 mm spacing to assess local softening and the width of the thermally affected region, i.e. heat affected zone.
Dataset and Experimental Coverage. The full experimental dataset, spanning all sheet thicknesses and DoE conditions, is shown in Fig. 4.

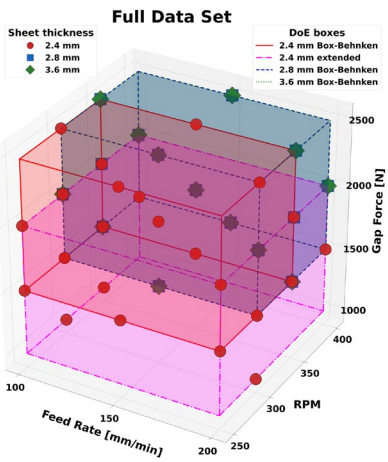

Fig.4 Full Data Set investigated for the different thicknesses.

The complete dataset comprises 61 individual welding conditions spanning three sheet thicknesses. It includes three Box–Behnken matrices corresponding to the 2.4, 2.8, and 3.6mm sheets, which together account for 45 structured welding conditions used for process analysis and mechanical validation. The remaining welds were produced after defining a feasible process window in order to improve coverage of the continuous parameter space and to ensure sufficiently sized training, validation, and test subsets for regression modeling; these supplementary points include both intermediate parameter combinations within the DoE space and selected combinations not coinciding with the original DoE design points, all of which lie within the mechanically validated process window. Each data point corresponds to a single weld and includes the process parameters and synchronized force measurements recorded during welding. The dataset is divided into training, validation, and test subsets containing 49, 6, and 6 welds, respectively. Sample selection for the validation and test sets is carried out such that all corresponding parameter combinations lie within the parameter bounds spanned by the training data, thereby fulfilling the defined interpolation criterion and avoiding extrapolative model evaluation. All three subsets maintain balanced representation across sheet thicknesses and process-parameter ranges, enabling an unbiased assessment of model generalization over the full BT-FSW operating window.

Data Acquisition and Pre-Processing. During welding, torque, rotational speed, traverse speed, and force signals in the x-, y-, and z-directions ($\mathbf{F_x}$, $\mathbf{F_y}$, $\mathbf{F_z}$) were recorded at a sampling frequency of approximately 70 Hz. The acquired signals were preprocessed to remove obvious outliers and were time-aligned across all channels using their common acquisition timestamps. To ensure consistency between welds, non-steady process segments corresponding to tool plunge, ramp-up, and termination were excluded from further analysis, in accordance with other works **[15]**. This preprocessing step ensured a consistent representation of the steady-state welding phase across all experiments.

Feature Engineering. The steady-state region of each weld was isolated by selecting the continuous time interval after tool entry and before termination in which the torque signal exhibited an approximately constant mean and low temporal variance, thereby excluding plunge, ramp-up, and termination. Thus, signals from this steady-state region were condensed into low-dimensional descriptors by computing statistical features and physically motivated force combinations, capturing the representative thermo-mechanical response during stable welding **[16]**. Normalized force components (e.g., Fx_norm, Fy_norm, Fz_norm) were defined by scaling the mean force components with the mean gap force to remove absolute load-level effects, while force ratios (e.g., Fx_Fz, Fy_Fz, Fxy_ratio) capture directional asymmetry between force components and force-interaction terms (e.g., FxFz, FyFz, FxFy) represent coupled loading effects acting simultaneously during welding. The resulting feature set comprises aggregated descriptors derived from process parameters (rotational speed, traverse speed, and gap force) and measured force signals, while the mean steady-state torque serves as the target variable for supervised regression. An overview of all extracted features is provided in Table 2.

Table 2 Overview of extracted features.

Category	Feature	Description
Process parameters	mean_rpm	Mean rotational speed (steady state)
Process parameters	mean_feed	Mean traverse speed
Process parameters	mean_gapforce	Mean gap force
Forces (statistical descriptors)	mean_fx, mean_fy, mean_fz	Mean force components
Forces (derived)	F_result	Resultant force magnitude
Force ratios	Fx_norm, Fxy_ratio	Normalized and directional ratios
Force interactions	Fx_Fz, Fy_Fz, FxFy, FxFz, FyFz	Coupled force terms
Parameter interactions	rpm_feed, rpm_gap, feed_gap	Physically motivated interaction terms

Machine Learning Models. The engineered features were used to train supervised regression models to predict the average steady-state torque. Linear regression was employed as an untuned baseline model, while Ridge regression was used to assess the effect of linear regularization. In addition, non-linear models—Random Forest, XGBoost, and CatBoost were applied to capture potential non-linear interactions between process parameters, force features, and torque **[17, 18]**. As mentioned above, the dataset was split at the weld level into training, validation, and test subsets. Hyperparameter optimization was performed exclusively on the training data using 5-fold cross-validation. For Ridge regression, the regularization parameter was optimized via a grid search over logarithmically spaced values. Random Forest hyperparameters, including the number of trees, maximum tree depth, and minimum samples per leaf, were likewise tuned using grid search. For XGBoost and CatBoost, Bayesian optimization based on a tree-structured Parzen estimator was employed to efficiently explore higher-dimensional hyperparameter spaces, including learning rate, tree depth, number of estimators, and regularization parameters. Model selection was based on predictive performance on the validation set, and the final selected models were subsequently evaluated on the independent test set to assess generalization performance.

Evaluation Metrics. Model performance was quantified using the mean squared error (MSE) and the coefficient of determination (R^2):

$$\mathbf{MSE} = \frac{1}{n}\sum_{i=1}^{n}(T_i - \hat{T}_i)^2$$

$$\mathbf{R^2} = 1 - \frac{\sum_{i=1}^{n}(T_i - \hat{T}_i)^2}{\sum_{i=1}^{n}(T_i - \bar{T})^2}$$

where n is the number of samples, T_i is, the measured steady-state torque of sample i, $\hat{T}_i$ is the corresponding predicted torque, and $\bar{T}$ is the mean of the measured steady-state torque values.

Mechanical and Microstructural Results

Tensile Properties Across Thicknesses. The tensile properties of all welded joints are presented in Fig. 5a–b. The base material exhibited ultimate tensile strength (UTS) of 432.1 ± 3.5 MPa, 450.4 ± 2.0 MPa and 454.9 ± 2.3 MPa for the 2.4-, 2.8- and 3.6-mm sheets, respectively, with yield strengths around 311–313 MPa and elongations of 16.3–18.1%. These base-material properties provide a quantitative reference for assessing the relative tensile properties and joint efficiency of the welded specimens.

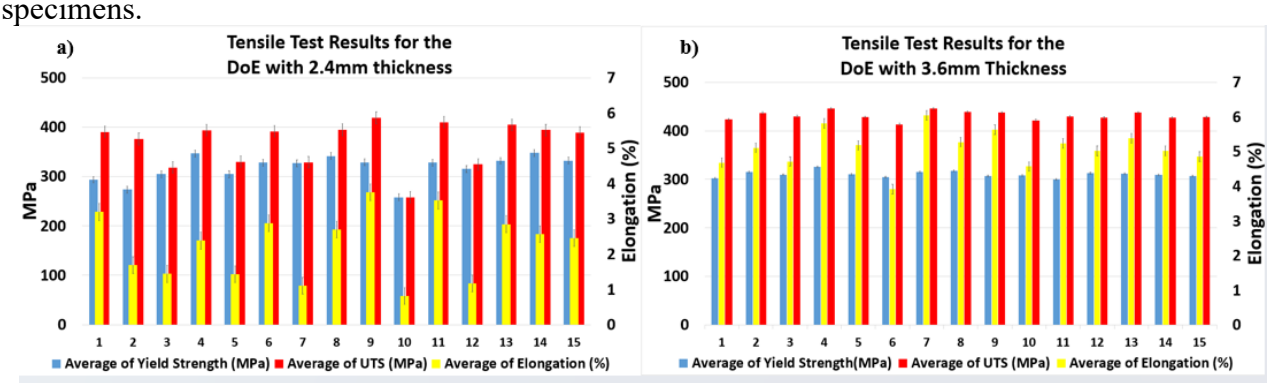

Fig. 5 Ultimate tensile strength comparison between thicknesses: a) 2.4mm; b) 3.6mm.

The 2.4 mm sheets exhibited the largest scatter in tensile strength, with UTS values ranging from approximately 258 MPa (~60% efficiency; Run 10: 350 rpm, 150 mm/min, 1500 N) to 419 MPa (~97% efficiency; Run 9: 300 rpm, 150 mm/min, 1500 N), see Fig. 5a). This wide variation reflects the high sensitivity of thin sheets to heat input fluctuations and localized flow instabilities, often associated with incomplete stirring or joint-line remnants during BT-FSW.

In contrast, the 2.8 mm sheets displayed improved consistency, with UTS values spanning from approximately 323 MPa (~72% efficiency; Run 7: 350 rpm, 200 mm/min, 1500 N) to 445 MPa (~99%

efficiency; Run 11: 300 rpm, 150 mm/min, 2500 N), indicating more homogeneous thermo-mechanical conditions at intermediate thickness.
The 3.6 mm joints showed the most stable behavior, with UTS values confined to a narrower range from approximately 422 MPa (~93% efficiency; Run 6: 350 rpm, 100 mm/min, 2500 N) to 446 MPa (~98% efficiency; Run 7: 350 rpm, 200 mm/min, 1500 N), see Fig. 5b). This enhanced stability reflects improved heat retention and more uniform material flow in thicker sheets.
Overall, weld stability increases with sheet thickness, with the 2.4 mm joints showing high sensitivity to parameter deviations and the 3.6 mm joints maintaining consistently high efficiency across DoE. Across all thicknesses, higher tensile strengths were obtained at moderate rotation speeds (≈300–350 rpm), intermediate traverse speeds (≈150 mm/min), and gap forces between 1500 and 2500 N, while combinations of high rotation speed or high traverse speed at low gap force led to reduced strength, highlighting the coupled influence of the process parameters.
Metallography. Microstructural observations reveal thickness-dependent stirring behavior. In the 2.4 mm welds, the etched sections show distinct joint-line remnants (JLR) within the nugget, Fig. 6, indicating incomplete interface disruption due to insufficient material flow in thin sheets with limited thermal inertia. Their presence correlates with the lowest tensile strengths and increased torque variability observed in the corresponding DoE runs.

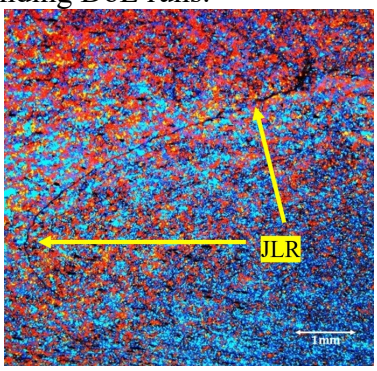

Fig.6 Joint Line Remnants in the nugget in the thickness of 2.4mm.

In contrast to the 2.4 mm joints, the 3.6 mm welds exhibit a uniformly consolidated stir zone at the macroscopic scale, as shown in Fig. 7. No joint-line remnants or interface-related discontinuities are observed across the nugget, indicating stable material flow and sufficient forging pressure in the thicker sheets. The absence of macroscopic defects is consistent with the high joint efficiency and reduced scatter observed in the mechanical properties for this sheet thickness.

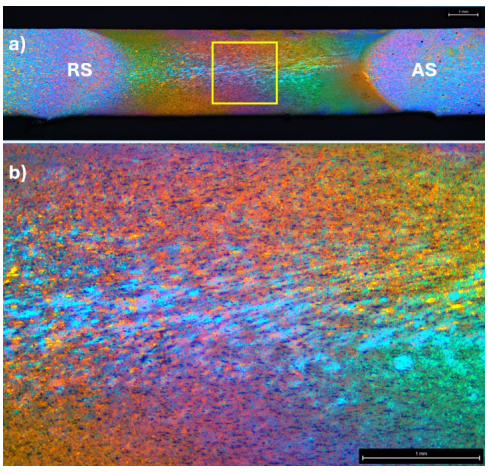

Fig. 7 Plan-view etched optical micrographs of the 3.6 mm BT-FSW weld confirming the absence of a joint line remnant (JLR); (a) global weld overview, (b) magnified central region showing continuous material flow across the weld center

Optimal Process Parameters. Parameter optimization reveals a clear thickness-dependent shift in the BT-FSW processing window. For the 3.6 mm sheets, the multi-response desirability analysis shown in Fig. 8 highlights a region of high combined mechanical performance, based on predicted yield strength (Rp0.2) and ultimate tensile strength (Rm), located around a rotational speed of approximately 400 rpm, a traverse speed of 200 mm/min, and a gap force of about 1500 N. The vertical red dashed lines in Fig. 8 denote the center points of the Box–Behnken design used for this thickness and serve as reference levels within the investigated parameter space, rather than indicating a unique optimal condition.

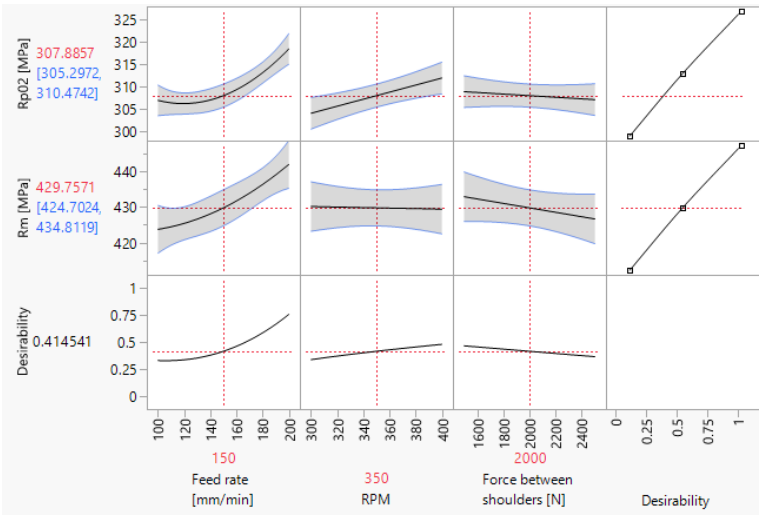

Fig. 8 Multi-parameter desirability analysis for BT-FSW specimens of 3.6 mm thickness, identifying the optimal combination of process parameters. Solid lines indicate the fitted responses for yield strength and ultimate tensile strength, while the shaded bands represent the 95% confidence intervals of the fitted models (JMP default).

For the 2.8 mm sheets, this favorable parameter region shifts toward lower rotational and traverse speeds and higher gap force, centered around 300 rpm, 150 mm/min, and 2000 N, whereas the 2.4 mm sheets exhibit a narrower region of stable operation near 250 rpm, 130 mm/min, and 2160 N, reflecting their reduced thermal inertia. Overall, increasing sheet thickness progressively broadens the stable operating window: thicker sheets allow a wider range of process parameter combinations, while thinner sheets require tighter coupling of rotational speed, traverse speed, and gap force, in agreement with established friction stir welding studies **[1]**.

Machine Learning Results

While the DoE and mechanical characterization establish thickness-dependent process windows and identify defect-free welding conditions, these results rely on destructive post-process testing and are therefore not directly accessible during welding. Torque, in contrast, is continuously measured during BT-FSW and reflects the instantaneous thermo-mechanical state of the process. However, its direct interpretation is non-trivial due to the coupled influence of process parameters, material thickness, and force response.

The purpose of the following machine-learning analysis is therefore not to replace the DoE-based findings, but to translate the mechanically validated process knowledge into a quantitative, signal-based model. By predicting steady-state torque from process parameters and force-derived features, a data-driven link is established between experimentally confirmed weld quality and in-process measurements.

Regression models trained using only nominal process parameters (rotational speed, traverse speed, and gap force), Fig. 9 a), exhibited markedly higher prediction errors compared to models augmented with force-derived features, Fig. 9 b), indicating that steady-state torque cannot be reliably inferred from programmed inputs alone.

Building on this enhanced feature representation, the performance of different regression algorithms was evaluated. Ordinary linear regression exhibited higher validation and test errors, reflecting its sensitivity to correlated process and force-derived features. Ridge regression yielded the lowest MSE on the validation set compared to all other models and was therefore selected as the best-performing model; the prediction performance on the test dataset was likewise superior based on the lowest achieved MSE, see Fig 9 b). This behavior is consistent with modelling principles indicating that linear methods generalize well when dominant physical effects are already encoded in the feature space **[20]**.

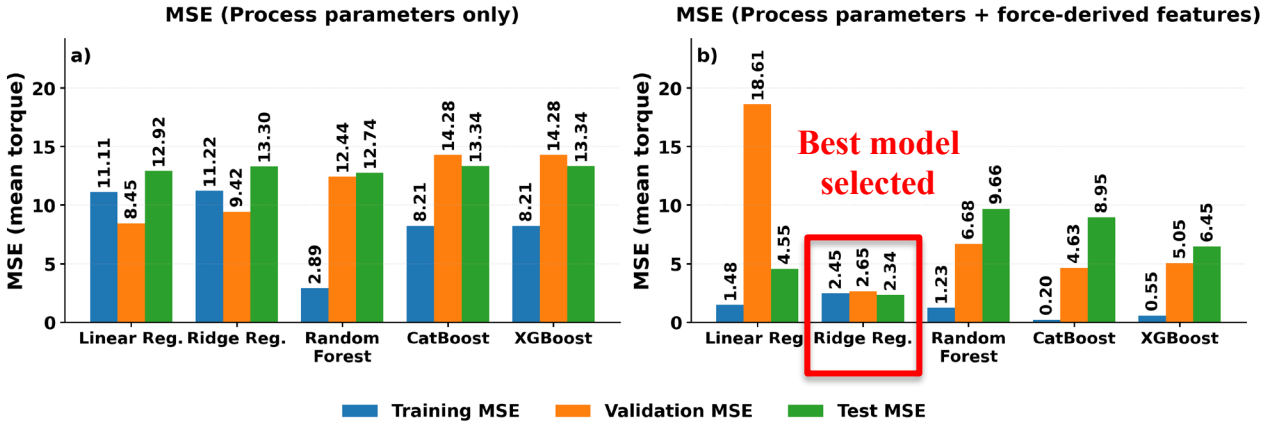

Fig. 9 Comparison of torque prediction accuracy for different models with different feature sets: (a) process parameters only, (b) process parameters with force-derived features.

Model agreement between predicted and measured torque across train/validation/test subsets is shown on Fig. 10.

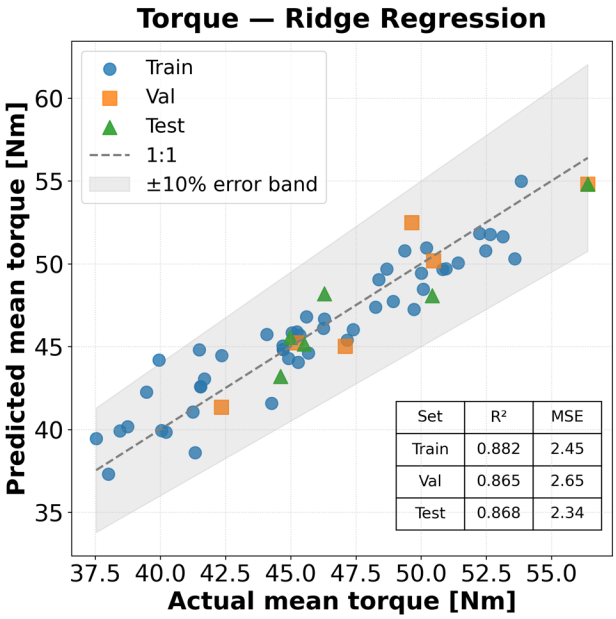

Fig.10 Ridge regression model: predicted vs. measured steady-state torque for train, validation and test sets.

Ensemble models such as Random Forest, XGBoost, and CatBoost captured additional nonlinearities but exhibited greater sensitivity to hyperparameter tuning and a mild tendency toward overfitting, as commonly observed for boosted-tree architectures **[21]**. Feature-importance analysis based on ridge regression coefficients (Fig. 11) identified rotational speed, vertical force magnitude, and parameter force interaction terms as the primary contributors to steady-state torque prediction.

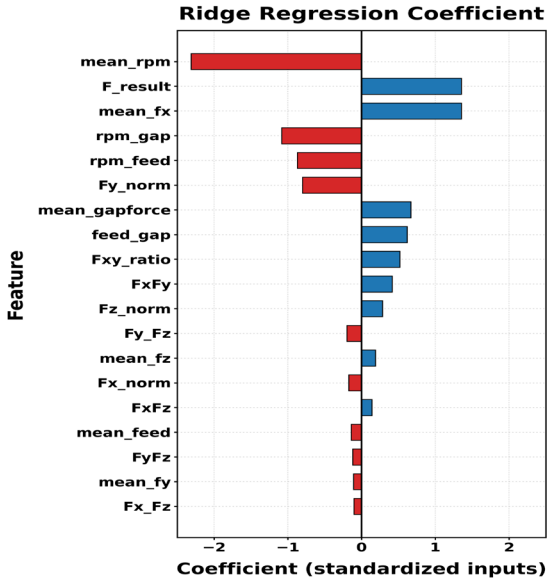

Fig. 11 Ridge regression coefficient ranking for torque prediction.

This ranking is consistent with established FSW mechanics, in which frictional heat generation, forging pressure, and material flow resistance jointly govern torque evolution during stable welding conditions **[1]**. Rotational speed and the resultant vertical force therefore emerge as dominant predictors, reflecting their direct influence on heat input, material plasticization, and resistance to tool motion. In contrast, normalized force components and force-ratio terms contribute at a secondary level, capturing more localized effects related to flow asymmetry and deviations from ideally uniform stirring.

In summary, the results show that accurate torque prediction in BT-FSW requires augmenting the nominal welding parameters with descriptors derived from the measured process forces. Once these engineered features were introduced, the regression framework achieved both high predictive performance and strong physical interpretability, consistent with physics-informed soft-sensor concepts reported in the literature **[10]**, where data-driven surrogate models guided by process mechanics demonstrated low prediction error and stable generalization within defined process windows, even under limited experimental data. The proposed approach therefore provides a reliable foundation for soft-sensing applications in BT-FSW, while not replacing the prior identification of suitable welding parameter windows, which remain essential for calibrating and validating the soft sensor.

Conclusions

A combined experimental and data-driven investigation of bobbin-tool friction stir welding of AA2024-T351 was performed across three sheet thicknesses. A structured DoE quantified the coupled influence of rotational speed, traverse speed, and gap force on weld morphology, tensile properties, and steady-state torque response. The mechanical results revealed a clear thickness dependence of process stability: 2.4 mm welds showed pronounced sensitivity to parameter variations and joint-line remnants, whereas 3.6 mm welds consistently achieved high joint efficiency with fully consolidated stir zones.

Building on these findings, a supervised regression-based soft-sensing framework was developed for steady-state torque prediction. Models relying solely on nominal process parameters were insufficient, while augmenting the input space with force-derived descriptors led to a substantial improvement in predictive accuracy. Ridge regression provided robust predictions together with physically interpretable feature rankings, with dominant contributors consistent with established friction stir welding results. Overall, the results demonstrate that compact, physically meaningful descriptors offer a viable and data-efficient route toward soft-sensing and process monitoring for bobbin-tool friction stir welding under limited experimental data availability.

Acknowledgements

The work was carried out under grant numbers 20X2206A and 20X2206G, funded by the German Federal Ministry of Economic Affairs and Energy (BMWE) under the LuFo VI-3 program.

References

[1] R. S. Mishra and Z. Y. Ma, "Friction Stir Welding and Processing," Materials Science and Engineering: R: Reports, vol. 50, no. 1–2, pp. 1-78, 2005.

[2] K. Fuse and V. Badheka, "Bobbin-Tool Friction Stir Welding: A Review," Journal of Manufacturing Processes, vol. 24, no. 4, pp. 277-304, 2019.

[3] J. S. Sashank, P. Sampath, P. S. Krishna, R. Sagar, S. Venukumar and S. Muthukumaran, "Effects of friction stir welding on microstructure and mechanical," Materials Today: Proceedings, vol. 5, no. 2, Part 2, pp. 8348-8353, 2018.

[4] R. R. Varma, A. B. Ibrahim, Mohammed and A. B. Mansor, "Mechanical properties of the friction stir welded dissimilar aluminium alloy joints," International Journal of Mechanical and Production Engineering, vol. 2, no. 5, pp. 1-5, 2014.

[5] A. C. Murariu, "Non-destructive and mechanical tests for quality evaluation of friction stir welding joints," Welding in the World, vol. 64, no. 5, p. 1005–1015, 2020.

[6] F. Nadeau, A. Cadiou, E. Feulvarch and M. Jahazi, "Machine-learning models applied to friction stir welding defect index using multiple joint configurations and alloys," Proceedings of the Institution of Mechanical Engineers, Part B: Journal of Engineering Manufacture, vol. 233, no. 10, p. 2535–2549, 2019.

[7] S. E. Belalia, M. Serier and R. Al-Sabur, "Parametric analysis for torque prediction in friction stir welding using machine learning and Shapley additive explanations," Journal of Computational Applied Mechanics, vol. 55, no. 1, p. 113–124, 2024.

[8] F. E. Bock, L. A. Blaga and B. Klusemann, "Mechanical performance prediction for friction riveting joints of dissimilar materials via machine learning," Procedia Manufacturing, vol. 47, p. 615–622, 2020.

[9] M. Penalva, A. Martín, C. Ruiz, V. Martínez, F. Veiga, A. G. d. Val and T. Ballesteros, "Application-Oriented Data Analytics in Large-Scale Metal Sheet Bending," Applied Sciences, vol. 13, no. 24, 2023.

[10] F. E. Bock, Z. Kallien, N. Huber and B. Klusemann, "Data-driven and physics-based modelling of process behaviour and deposit geometry for friction surfacing," Computer Methods in Applied Mechanics and Engineering, vol. 418, 2024.

[11] W. Homberg, B. Arian, V. Arne, T. Borgert, A. Brosius, P. Groche, C. Hartmann, L. Kersting, R. Laue, J. Martschin, T. Meurer, D. Spies, A. E. Tekkaya, A. Trächtler, W. Volk, F. Wendler and M. Wrobel, "Soft sensors: key component of property control in forming technology," Production Engineering, vol. 18, no. 3-4, p. 603–614, 2024.

[12] D. A. Efa, E. M. Gutema, H. G. Lemu and M. Gopal, "Friction stir-welding of AZ31B Mg and 6061-T6 Al alloys optimization using Box-Behnken design (BBD) and artificial neural network (ANN)," Research on Engineering Structures and Materials, vol. 10, no. 1, p. 413–430, 2024.

[13] H. Aydın, A. Bayram, A. Uğuz and K. S. Akay, "Tensile properties of friction stir welded joints of 2024 aluminum alloys in different heat-treated state," Materials & Design, vol. 30, no. 6, p. 2211–2221, 2009.

[14] F. Wang, W. Li, J. Shen, S. Hu, J. Li, J. d. Santos and N. Huber, "Effect of tool rotational speed on the microstructure and mechanical properties of bobbin tool friction stir welding of Al-Li alloy," Materials & Design, 2015.

[15] S. Bag, S. Pal and S. Bose, "Monitoring of friction stir welding process through signals acquired during the welding," in Proceedings of the AIMTDR (All India Manufacturing Technology, Design and Research Conference), 2014.

[16] A. Astarita, A. Squillace and L. Carrino, "Experimental study of the forces acting on the tool in the friction stir welding of AA2024-T3 sheets," Journal of Materials Engineering and Performance, vol. 23, p. 3754–3761, 2014.

[17] A. V. Dorogush, V. Ershov and A. Gulin, "CatBoost: Unbiased boosting with categorical features," in Advances in Neural Information Processing Systems (NeurIPS), 2018.

[18] T. Chen and C. Guestrin, "XGBoost: A scalable tree boosting system," ACM Transactions on Intelligent Systems and Technology, vol. 7, no. 3, 2016.

[19] T. Hastie, R. Tibshirani and J. Friedman, "The Elements of Statistical Learning: Data Mining, Inference, and Prediction," Springer Series in Statistics, p. 1–745, 2009.

[20] J. H. Friedman, "Greedy Function Approximation: A Gradient Boosting Machine," The Annals of Statistics, vol. 29, no. 5, p. 1189–1232, 2001.

[21] A. Forcellese, M. Simoncini and G. Casalino, "Influence of process parameters on the vertical forces generated during friction stir welding of AA6082-T6 and on the mechanical properties of the joints," Metals, vol. 7, no. 9, 2017.